QUARTERLY JOURNAL OF THE ROYAL METEOROLOGICAL SOCIETY
Q. J. R. Meteorol. Soc. **135**: 67–75 (2009)
Published online 3 December 2008 in Wiley InterScience
(www.interscience.wiley.com) DOI: 10.1002/qj.348

Space–time structure of mesoscale motions in the stable boundary layer

L. Mahrt,[a]* C. K. Thomas[a] and J. H. Prueger[b]
[a] *COAS, Oregon State University, Corvallis, OR 97331, USA*
[b] *USDA-ARS, National Soil Tilth Laboratory, Ames, IA 50011, USA*

ABSTRACT: In this article, we examine the stochastic characteristics of non-turbulent motions in the stable boundary layer. The behaviour of mesoscale motions in the atmospheric stable boundary layer is poorly understood beyond case studies of unusually well-defined events or monotonic waves. Eight networks of wind observations are analysed in order to examine stochastically the space–time characteristics of such motions in the stable boundary layer. The networks include a variety of surface conditions and network configurations, although none of the networks is optimal for our studies. Collectively, the networks allow examination of scales from tens of metres to tens of kilometres.
A variety of analysis tools reveal the complexity of mesoscale motions near the surface in stratified flow. For the data as a whole, the horizontal scale of coherence increases systematically with time-scale, albeit with large scatter between records. The relationship between spatial coherence and time-scale is posed in terms of a velocity scale, which is found to be unrelated to the wind speed. The time variability of the flow decreases systematically with increasing spatial averaging, suggesting that comparison of model winds (with implied spatial averaging over the grid area) with observations requires suitable spatial averaging of the observations. Additional characteristics are discussed in terms of non-dimensional ratios of velocity scales. Necessary improvements of network measurements are also noted. Copyright © 2008 Royal Meteorological Society

KEY WORDS stable boundary layer; nocturnal boundary layer; mesoscale; stratified flow

Received 19 May 2008; Revised 15 October 2008; Accepted 27 October 2008

1. Introduction

In some sense, mesoscale motions in stable boundary layers are more complicated than turbulence. The mesoscale motions simultaneously include a variety of generating mechanisms (see references in Mahrt, 2007), which apparently precludes spectral similarity theory. This contrasts with mesoscale motions above the boundary layer where a constant spectral slope is observed (e.g. Lilly, 1983; Lindborg, 1999). 'Small' mesoscale motions on scales just larger than the turbulence for stable conditions may extend down to horizontal scales of the order of 10 m and time-scales of a minute or less, and may sometimes be confined to layers of a depth of only a few metres. These motions are on scales smaller than what is typically included in the term 'mesoscale'. We arbitrarily refer to such non-turbulent motions as 'submeso' scale motions. Admittedly, the statistical characteristics and complex physics may vary continuously from the turbulence scale to the submeso and larger mesoscales, without well-defined scale separation. Here, 'mesoscale' is used loosely to cover the entire range of scales including the submeso motions.

Mesoscale motions often propagate with different directions and speeds than the mean wind (e.g. Rees *et al.*, 2000) and show little relationship to local scaling variables (e.g. Vickers and Mahrt, 2007). Mesoscale motions in stable boundary layers can be generated by even weak surface heterogeneity and modest terrain slopes, leading to site dependency. Multiple generation mechanisms, and resulting erratic variation of the kinetic energy with scale and between records, precludes development of meaningful similarity theory for most sites. Collectively, these complications prevent definition of an ensemble average and the attendant support of statistical theories for random processes.

In order to partially understand the physics of such motions, previous studies have concentrated on special cases of simplified flows, such as density currents, monotonic gravity waves and solitons (e.g. Finnigan, Einaudi and Fua, 1984; Rees, Anderson and King, 1998; Nappo, 2002; Anderson, 2003; Sun *et al.*, 2004). The majority of the data records from fast response anemometers appear more chaotic, even if one or two cycles of waves can be frequently identified (Nakamura and Mahrt, 2005). Even gravity waves alone can be quite complex (e.g. Shutts, 1998). The relative roles of complex phenomena, in contrast to the complex superposition of simple signatures, are not known. Mesoscale motions include both linear wave-like phenomena and frequent

*Correspondence to: L. Mahrt, COAS, Oregon State University, Corvallis, OR 97331 USA. E-mail: mahrt@coas.oregonstate.edu

highly nonlinear structures with near discontinuities, such as microfronts (Mahrt, 2008). Mesoscale motions on scales of kilometres or more can include horizontal meandering motions (e.g. Hanna, 1983; Anfossi *et al.*, 2005).

Spatial structure is often inferred from time series by invoking Taylor's hypothesis. However, this hypothesis is not valid even as a first approximation for meso motions, which often propagate with a speed and direction that is quite different from the mean wind vector. Aircraft data provide good spatial resolution, but only nominal time sampling at a fixed point (repeated passes), and aircraft data availability in the stable boundary layer is quite limited. Hanna and Chang (1992) used a network of anemometers to determine the decrease of correlation between stations with increasing separation distance and the dependence of this decrease on averaging time. Applying multiple statistical approaches to three networks of fast response data, Belušić and Mahrt (2008) found a preferred horizontal scale of several kilometres, which varied between the networks.

In this article, we incorporate data from eight non-urban networks and extend the spatial analysis of Belušić and Mahrt (2008). While these networks provide new statistical information, the spatial resolution is much more coarse than the time resolution provided by the anemometers. Thus, the examination of the space–time relationships of meso motions are not symmetric in space and time, and formal joint decompositions into space and time have been determined to be not well posed. Here, we orthogonally decompose the motions into different time-scales and then examine the spatial coherence of each time-scale.

2. Data

The eight networks include a variety of domain sizes (Table I) and cover a variety of surface types and climatologies. The CASES99, EBEX, Mary's River, Mature Pine and Young Pine sites all interrogate scales less than 1 km, within the submeso range. The data periods are restricted to summer and early autumn, except for the Hereford network (Hanna and Chang, 1992) operated in the spring. Each network has unique advantages and difficulties. All of the datasets would benefit from greater sample size. The Utah network covers the largest area and resolves more traditional mesoscales of the order of 10 km or more, but has only 5 min time resolution. The rest of the networks include at least 1 min time resolution. In this article, we emphasize the Iowa network, which is the most favourable in terms of uniform surface conditions, minimal terrain and adequate domain size. Data are analysed from 2000 to 0600 local standard time. The heights of the sensors vary from 10 m in the Utah and Hereford networks to 5 m for CASES99 (Poulos *et al.*, 2001) and EBEX (Oncley *et al.*, 2007), 2 m above the crops for the Iowa network (Kustas *et al.*, 2004) and 1 m above the understory for the Mary's River (Thomas *et al.*, 2008), Mature Pine (Schwarz *et al.*, 2004) and Young Pine (Schwarz *et al.*, 2004) networks.

Table I. Field programs. Network name, vegetation, number of stations, domain width (km), defined as the maximum distance between stations, and the duration of the dataset in months.

Site	Surface	Stations	Width	Duration
CASES99	Grass	7	0.6	1
EBEX	Cotton	8	1.0	1
Hereford	Grass	13	14	0.5
Iowa	Crops	9	11	0.75
Mary's River	20 m fir	7	0.1	4
Mature Pine	15 m pine	7	0.5	2.5
Utah	Semi-arid	22	100	1
Young Pine	3 m pine	9	0.2	4

Based on the CASES99 tower, the overall statistics of mesoscale horizontal velocity variations generally change only slowly with the height of the instruments, even though the height dependence may be large for individual cases. The Hereford and Utah networks used propellor anemometers. The other networks used three-dimensional or two-dimensional sonic anemometers. The Utah network consists of 26 stations with R. M. Young Model 05103 anemometers with an accuracy of 0.3 m s^{-1} and an official startup threshold of 1.0 m s^{-1}, although the actual threshold appeared to be significantly less. Surface vegetation consists primarily of sparse semi-arid grasses and bushes, which were mostly senescent during the observational period. Nominal quality control was applied to all of the datasets to remove occasional spikes.

The three eastern stations in the Iowa domain contain substantial missing data and are eliminated, leaving nine stations. For all of the networks, we have computed statistics for a subset of records when all stations are available. These statistics were close to the original statistics for all of the networks, and in this article we report only the original statistics. The statistics must be interpreted with caution, as observations of mesoscale motions do not allow formal estimation of ensemble averages, partly because the forcing mechanisms are varied and generally of unknown origin.

Because the structures in the records are generally local and not periodic over a significant fraction of the record, we orthogonally decompose the flow into the local multiresolution basis set (e.g. Howell and Mahrt, 1997; Skelly, 2004). The multiresolution basis set is the simplest possible wavelet basis set based on decomposition of the flow into unweighted averages over subrecords of different dyadic widths (2^n). It is the only decomposition that satisfies Reynolds averaging independently at all scales. An arbitrary variable ϕ for the ith record can be written as the sum of M multiresolution modes:

$$\phi(i) = \frac{1}{M}\sum_{1}^{M}\phi_m(i). \qquad (1)$$

DOI: 10.1002/qj

We apply the decomposition to 1 min averaged data, corresponding to multiresolution time dyadic scales of 1, 2, 4, 8, 16, 32 and 64 min. This requires 64 min records, which are constructed by overlapping records by 4 min in order that each record starts at the beginning of the hour. The statistics for the entire dataset are not detectably affected by this overlap. The 1 min averaging is chosen based on the observation that the turbulent time-scales rarely exceed 1 min for stable conditions, where the range of turbulent scales was determined as in Vickers and Mahrt (2006).

3. General measures of time and space variability

To contrast the different networks, we define several velocity scales based on time and space variability. The statistics of the mesoscale motions vary between networks because of different surface conditions, topography, climatology of the large-scale flow, and the size of the domain and spatial configuration of the stations. The results below reveal large differences between networks and emphasize the difficulty of making general conclusions on the behaviour of mesoscale motions.

We define a measure of the spatial variability of the flow for the ith record as

$$V_{\mathrm{Domain}}(i) \equiv \left\langle (\tilde{u}_{i,k}^2 + \tilde{v}_{i,k}^2)^{0.5} \right\rangle. \tag{2}$$

Here, the tilde represents the deviation of the 1 min value for station k from the 1 min spatial (network) average and the angle brackets indicate averaging over the stations in the network. We then average over all of the records to obtain $[V_{\mathrm{Domain}}]$ where the square brackets indicate averaging over all of the nocturnal records. The values of $[V_{\mathrm{Domain}}]$ (Table II, column 2) vary by an order of magnitude. The value of $[V_{\mathrm{Domain}}]$ is largest for the Utah domain, possibly because of its larger size and the influence of a complex terrain. Larger networks capture a larger range of mesoscale motions. Statistics were also computed for different parts of the large Utah network. The values of $[V_{\mathrm{Domain}}]$ for these subdomains were found to be smaller than those for the entire network. $[V_{\mathrm{Domain}}]$ is smallest for the subcanopy networks where the wind itself is weak and the network sizes are small.

The spatial variability is a result of transient mesoscale motions and spatial variation associated with surface heterogeneity, microsetting of the instruments and possible unknown instrument bias. Rather minor surface features, which would be of little consequence in the daytime heated boundary layer, can significantly influence stably stratified flow. Here, transient motions refer to variations on time-scales between 1 min and 1 h. The systematic time-independent spatial variation, V_{clim}, is computed from flow components that are first averaged over the entire data set:

$$V_{\mathrm{clim}} \equiv \left\langle [\tilde{u}_{i,k}]^2 + [\tilde{v}_{i,k}]^2)^{1/2} \right\rangle. \tag{3}$$

Here, again, square brackets indicate averages over all of the nocturnal records. The wind components averaged over the dataset vary systematically across the Utah, Mary's River and Mature Pine domains, corresponding to coherent heterogeneity on the domain scale. The time-averaged spatial variation is disorganized for the Iowa network, and disorganized and weak for the Hereford and EBEX networks. For these sites, the main heterogeneity is on scales smaller than the station spacing. Intermediate behaviour is observed for the remaining networks.

Table II. Nocturnal statistics. Statistics for the entire nocturnal dataset: the spatial variability of the 1 min averages, subsequently averaged over the dataset, $[V_{\mathrm{Domain}}]$ (m s^{-1}; see (2)), abbreviated as $[V_{\mathrm{D}}]$; the scaled spatial variability based on velocity components averaged over the entire dataset, *CR* (3); the fraction of the spatial variability due to time-scales between 1 min and 1 h, *R* (5); the ratio of time variability to space variability, *RT* (7); the ratio of time variability of the spatial average to the spatial average of the time variability at the individual stations, *RS* (8).

Site	$[V_{\mathrm{D}}]$	*CR*	*R*	*RT*	*RS*
CASES99	0.38	0.56	0.56	0.85	0.85
EBEX	0.57	0.33	0.29	1.13	0.82
Hereford	1.28	0.20	0.39	0.96	0.66
Iowa	0.78	0.49	0.29	0.54	0.62
Mary's River	0.42	0.73	0.37	0.71	0.77
Mature Pine	0.70	0.38	0.19	0.61	0.52
Utah	3.20	0.39	0.11	0.39	0.30
Young Pine	0.22	0.39	0.49	1.06	0.75

The relative importance of this time-invariant spatial variation is represented as

$$CR \equiv \frac{V_{\mathrm{clim}}}{[V_{\mathrm{Domain}}]}. \tag{4}$$

This ratio averages 0.43 over the eight networks, indicating that almost half of the spatial variation is associated with time-invariant spatial variation, the rest being associated with transient motions. The relative importance of time-independent spatial variability is greatest for the subcanopy Mary's River network (Table II) where winds are weak and spatial variations of understory and drainage flows are significant. This ratio is smallest for the relatively uniform Hereford grassland where the spatial variation appears to be associated primarily with the large transient variations.

A measure of the contribution of the time-scales between 1 min and 1 h to the total spatial variability is defined as

$$R \equiv \frac{[V_{\mathrm{Domain}}(\mathrm{min})] - [V_{\mathrm{Domain}}(\mathrm{h})]}{[V_{\mathrm{Domain}}(\mathrm{min})]}, \tag{5}$$

where V_{Domain} (h) corresponds to the spatial variability of the 1 h averaged flow. For the Young Pine and CASES99 networks, approximately half of the spatial variability is associated with time-scales of 1 min to 1 h (R; see Table II); the rest of the variance is associated with time-scales greater than 1 h, which includes the time-invariant part. The important contribution of time-scales less than 1 h to

DOI: 10.1002/qj

the spatial variability for the Young Pine and CASES99 networks is partly a result of the relatively invariant synoptic situation. For the rest of the networks, more of the spatial variability is associated with time-scales greater than 1 h and R is smaller (Table II).

We define a bulk measure of time variability for the ith record as

$$V_{\mathrm{Meso}}(i,k) \equiv (\overline{u*_{i,k}^2 + v*_{i,k}^2})^{0.5}, \tag{6}$$

where the overbar indicates a time average over the 1 h period and the asterisk signifies a 1 min time deviation from the record (1 h) average for a given station. As a measure of the relative importance of the time variability to the spatial variability, we compute

$$RT \equiv \frac{[\langle V_{\mathrm{meso}}\rangle]}{[V_{\mathrm{Domain}}]}, \tag{7}$$

where both quantities are based on the 1 min averages and the angle brackets on the right-hand side again indicate an average over the network domain. The Young Pine, CASES99, EBEX and Hereford networks are characterized by large time variability compared to spatial variability (Table II), partly related to the small domain size (more restricted range of spatial scales). With larger domain size, spatial variability becomes larger than the time variability, as observed with the Iowa and Utah domains.

The impact of spatial averaging on the time variability is computed as a ratio of the time variability of the spatial average to the spatial average of the time variability at the individual stations:

$$RS \equiv \frac{[\mathrm{V}_{\mathrm{meso}}(\langle\,\rangle)]}{[\langle V_{\mathrm{meso}}\rangle]}. \tag{8}$$

Here, the numerator is computed from the spatially averaged 1 min velocity components and the denominator is the spatial average of V_{meso} for individual stations. Values of RS less than unity indicate that spatially averaged flow is significantly less variable in time than the flow at the individual stations. For the largest domain (Utah), spatial averaging reduces the time variability by more than half (Table II). For the smaller networks such as the CASES99, EBEX, Young Pine and Mary's River networks, the spatial averaging reduces the time variability by 15–30%. For a given network size, the spatial averaging reduces the time variability within the subcanopy more than above the canopy because variability occurs on smaller spatial scales in the subcanopy. The influence of spatial averaging on time variability is discussed in more detail in Section 5.

The large variability between networks is partly a result of different network sizes. However, much of the difference cannot be explained in terms of network size, as is evident from inspection of Table II and supported by computing statistics for smaller subdomains of the large Utah network.

4. Dependence of spatial coherence on time-scale

In this section we examine the horizontal scale of coherence for motions on different time-scales for the entire nocturnal dataset. The large variation between the 1 h records is documented in Section 6. The correlation for a given wind component between two stations is computed for each multiresolution mode (each time-scale). The two-point correlation coefficients for the u- and v-components are combined as

$$R_{uv}(r) \equiv [(R_u^2 + R_v^2)/2]^{0.5}. \tag{9}$$

Here, R_u and R_v are the between-station correlation coefficients for the individual velocity components and r is the distance between stations. Information on the sign of the correlation is lost in this combination, which provides only the magnitude of the overall correlation. Scaling by 2 ensures that R_{uv} ranges between 0 and 1. Using all of the possible combinations of stations pairs and posing the analysis in terms of the separation distance, the two-dimensional dependence in the horizontal domain (x, y) collapses on to a one-dimensional dependence on r. The correlation coefficients for the along-wind and cross-wind flow did not show systematic differences, probably because the mesoscale motions are not strongly affected by wind direction. This contrasts with turbulent scales where higher correlation coefficients extend to larger separation distance in the along-wind direction compared to the cross-wind direction (King, 1988).

4.1. Iowa network

The between-station correlation coefficient for the Iowa network decreases with increasing separation distance and this decrease occurs at larger separation distances for larger time-scales (Figure 1). A similar dependence of the two-point correlation on separation distance is found for the other networks (Figure 2), as discussed in Section 4.2. The scatter is large probably because of the multiple physical influences on the mesoscale motions and the inadequacy of the data networks. The correlation coefficient for the 1 min mode, is comparable to, or less than, 0.1 even at the smallest separation distances of a few hundred metres. Evidently, the spatial scale of the 1 min mode is less than a few hundred metres and is not captured by the network grid. The asymptotic approach of the correlation to unity with vanishing separation distance becomes primarily governed by the turbulence velocity fluctuations on scales of seconds or tens of seconds, outside the scope of this study. At the other limit, the 64 min modes (record averages) maintain high correlations even for the largest separation distances of about 20 km. Therefore, the 64 min mode is significantly influenced by scales larger than a few tens of kilometres.

Simple exponential decay is an inadequate approximation to the decrease of between-station correlation with increasing separation distance, perhaps emphasizing that the mesoscale variations cannot be described by a simple random process (Yaglom, 1973). A better approximation

DOI: 10.1002/qj

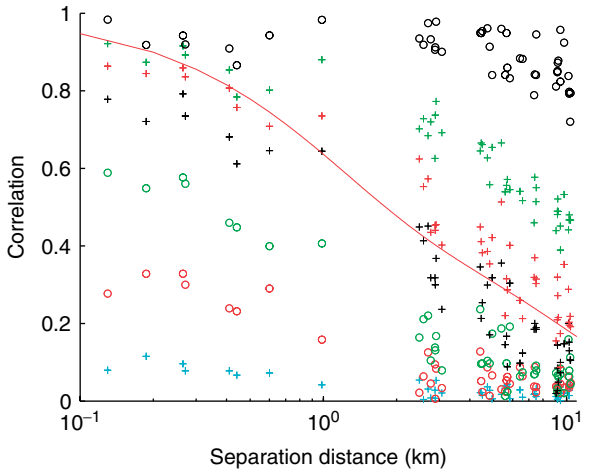

Figure 1. The dependence of between-station (two-point) velocity correlations in the Iowa network on station separation distance for different decomposition time-scales: 1 min (cyan crosses); 2 min, (red circles); 4 min (green circles); 8 min (black crosses); 16 min (red crosses); 32 min (green crosses) and 64 min (black circles). The 64 min mode corresponds to the record averages. The red line represents a fit for the 16 min mode based on (10).

to the data is provided by a double exponential function (two adjustable coefficients)

$$R_{uv} = a\exp(-r/R1) + (1-a)\exp(-r/R2), \qquad (10)$$

where r is the separation distance between two stations and $R1$ and $R2$ are horizontal length-scales. The 16 min mode in Figure 1 is approximated by $a = 0.5$, $R1 = 1$ km and $R2 = 10$ km. The second exponential term was added by Hanna and Chang (1994) and also applied by Belušić and Mahrt (2008). Although in this study we evaluate (10) independently for each time-scale, even two terms in the fit are often inadequate. Like Hanna and Chang (1994), we forego attempting to include more than two adjustable coefficients. In the mesoscale range, the interpretation of the two terms is uncertain. Exponential decay cannot be interpreted in terms of an integral scale because of fundamental difficulties with such a scale (e.g. Panofsky and Dutton, 1984; Treviño and Andreas, 2006). The fit in Figure 1 is for reference only and is not recommended for categorical application.

4.2. Other networks

The two-point correlation coefficient decays with increasing separation distance in a more regular fashion for some of the other networks (Figure 2). The space–time relationships vary significantly between networks, again emphasizing the non-universal behaviour of the mesoscale motions and possible dependence on surface conditions, prevailing synoptic conditions and network configuration. The two-point correlation coefficients become quite small for separation distances greater than 10 km in the Utah network, partly because of the lack of activity on larger spatial scales for time-scales less than 1 h, and possibly because of horizontal decoupling in the nocturnal boundary layer associated with a complex terrain. The decay of the two-point correlation coefficient with increasing separation distance is noisier for the subcanopy Mary's River and Mature Pine networks (not shown), probably because of the irregular understory and intermittent invasion of drainage flow into part of the network. In the latter case, the correlation between stations is related more to whether the two stations are in the same flow

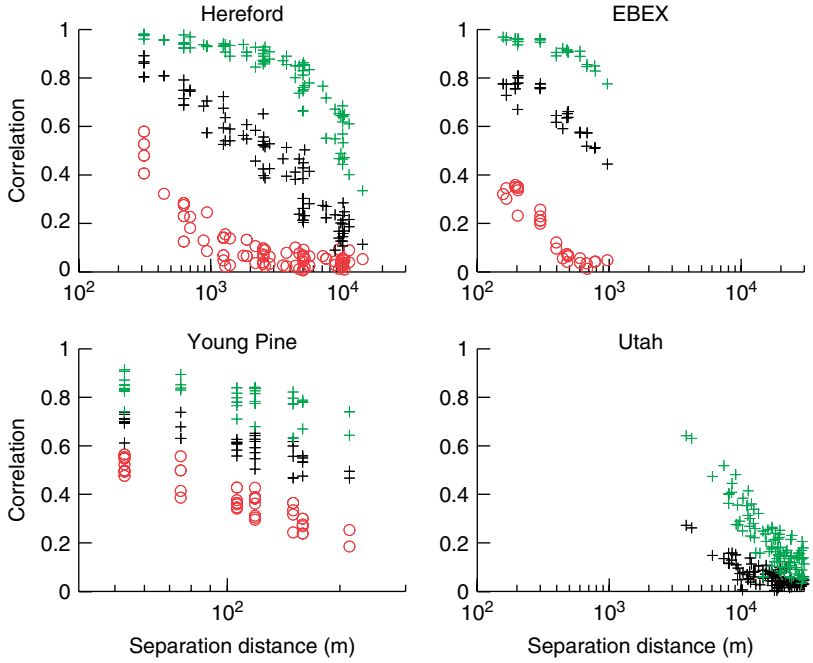

Figure 2. The dependence of between-station (two-point) velocity correlations on station separation distance for different decomposition time-scales: 2 min (red circles), 8 min (black crosses) and 32 min (green crosses) modes for the Hereford (a), EBEX (b), Young Pine (c) and Utah (d) networks. The Young Pine network is within a canopy with smaller horizontal scales and is therefore plotted for a smaller range of horizontal scales. The 2 min mode is not shown for Utah as the time resolution of the data is only 5 min.

DOI: 10.1002/qj

regime than to the actual separation distance between stations.

4.3. Decay rate

Although the decay of the correlation coefficient with separation distance is not well approximated with a single exponential decay, we can arbitrarily define a horizontal length-scale, L_e, where the two-point correlation has decreased to $1/e$. Here, the value of L_e was determined subjectively from the plots (e.g. Figure 2). Similar results were obtained with objective fits using two adjustable parameters, although the fits are sometimes of marginal statistical significance. More data are required. For the three networks with the largest range of horizontal scales (Figure 3), L_e increases systematically with increasing time-scale. A crude subjective fit for the three networks is

$$L_e = VM\,\tau, \tag{11}$$

where the velocity scale $VM \approx 8.3$ m s^{-1} (Figure 3, straight line) and τ is the time-scale. The fit could be improved significantly with a more complex function and network-dependent coefficients. This is not the purpose here. Of more importance, this velocity scale is much larger than the average wind speed, which is 1.8 m s^{-1} for the Iowa network, 3.6 m s^{-1} for the Utah network and 4.8 m s^{-1} for the Hereford network. Some disturbances could be propagating with the stronger wind at higher levels. However, animations of the wind field revealed that the propagation of mesoscale structures, when definable, was not closely related to the direction of the wind. *VM* does not have a detectable relation to the wind vector or an obvious physical interpretation. It is a stochastic quantity that roughly describes the increase of the horizontal length-scale with increasing time-scale. In conclusion, Taylor's hypothesis is not valid even as a first approximation, and case studies are required before attempting to explain the large value of *VM*.

4.4. Between-network comparisons for a given time-scale

The between-network comparison of the two-point velocity correlations for a given time-scale, here 8 min (Figure 4), indicates that the coherence between stations decreases with increasing separation distance in a similar manner for all of the networks. The main exception is that correlations are smaller for the Young Pine network, which consists of subcanopy data and is strongly influenced by an upstream roughness change. For the 8 min mode, the between-station correlation decreases to negligible values for separation distances greater than about 10 km, because of minimal activity on larger spatial scales.

4.5. Structure function

The two-point structure function includes information on the strength of the velocity differences as well as correlation. Scaling variables for constructing a non-dimensional structure function for mesoscale similarity theory have not been identified. Consider the dimensional two-point, second-order, velocity structure function for each time-scale summed over the dataset

$$S_u(k,l) = \frac{1}{I}\sum_{i}^{I}(u_{i,k} - u_{i,l})^2, \tag{12}$$

where u_k and u_l are the wind components in the x-direction for stations k and l, separated by distance r. S_v is computed in an analogous way. The magnitude of the two-component velocity structure function is computed as

$$S \equiv (S_u^2 + S_v^2)^{0.5} \tag{13}$$

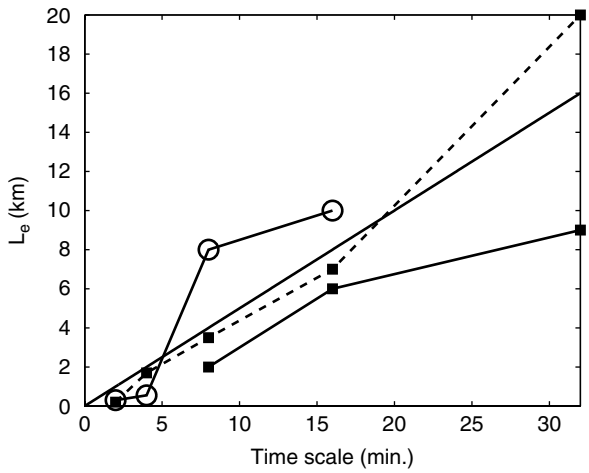

Figure 3. The dependence of the horizontal length-scale, L_e, on time-scale for the three networks with the largest range of spatial scales: Iowa (dashed line), Hereford (solid line, open circles) and Utah (solid line). For reference, the straight line corresponds to an increase of horizontal scale with increasing time-scale at a rate of 8.3 m s^{-1}.

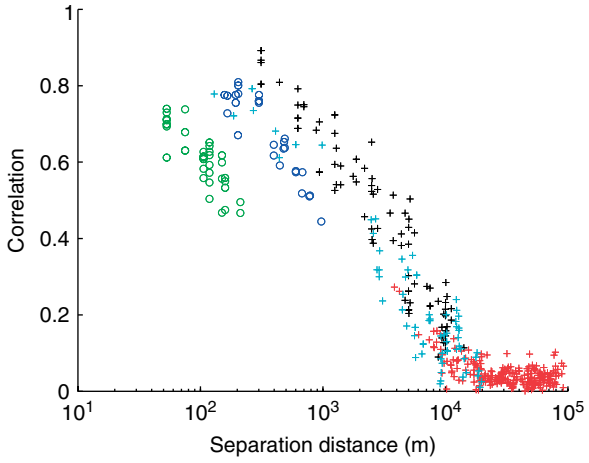

Figure 4. The dependence of between-station (two-point) velocity correlations on station separation distance for the 8 min mode for the Young Pine (green circles), Utah (red crosses), EBEX (blue circles), Iowa (cyan crosses) and Hereford (black crosses) networks.

DOI: 10.1002/qj

for each station pair and time-scale. For the Iowa network, the velocity structure function for the 1 min time-scale (Figure 5, black circles) has already approximately reached its maximum value at the smallest separation distances of a few hundred metres, indicating that motions on the 1 min time-scale are primarily on space-scales smaller than a few hundred metres (i.e. smaller than that resolved in the densest part of the network). In contrast, the structure function for the 32 min time-scales (Figure 5, red crosses) increases rapidly with increasing separation distance for separation distances between about 2 and 20 km; motions on these horizontal scales contribute significantly to the 32 min structure function. Recall that each record contains only two samples of the 32 min mode, but each point in Figure 5 represents an average over the entire dataset.

At the smallest separation distances, the 32 min mode has less variance than the 1 min mode because the small separation distance misses most of the spatial variation associated with the 32 min mode. The behaviour of the structure function is not pursued further as scaling to a non-dimensional form is not available.

5. Dependence of time variability on spatial averaging

In the above analyses, we have examined the dependence of spatial coherence on averaging time. The symmetric analysis of the time coherence for different space-scales is not possible to the same degree because the station spacing is too crude and variable. However, we can examine the dependence of the time variability on spatial averaging.

The ratio of the time variability after spatial averaging over the domain, to that before spatial averaging, RS, decreases systematically with increasing domain size (Figure 6), where we have excluded the within-canopy networks. The reduction of time variability based on 1 min averages (filled circles) is greater than that based on 10 min averages (asterisks) because larger time-scales are statistically associated with larger space-scales and less affected by spatial averaging. However, the difference between the two averaging times is only about 10%. For reference, the solid line in Figure 6 corresponds to an exponential decay with a $1/e$ folding length of 50 km. A more complex function is required, but its construction must wait for additional data. The degree of generality of Figure 6 is not known as the dependence of time variability on spatial averaging may depend on synoptic conditions, surface character and topography.

The reduction of time variability by spatial averaging is important when comparing observations with numerical models, where spatial averaging over a grid box is implied. That is, observations at a point will vary more in time than spatially averaged variables. As a rough example of the $1/e$ decay relationship, the evaluation of a model with horizontal grid spacing of 10 km would require a reduction of the observed time variability at a fixed station by about 20%. Preferably, models can be directly compared with observations averaged over a suitable spatial domain similar to the size of the grid-box area.

6. Space–time relations for individual records

The spatial coherence for a given time-scale varies substantially between records. Consider two classes of large deviations from the 'average' space–time relationship, revealed by animations of the wind field and schematically recorded in terms of time- and space-scales in Figure 7. The lower-right corner of Figure 7 corresponds to fast moving large structures characterized by large horizontal scales, but small time-scales observed at a fixed point. Conversely, in the upper-left corner, slowly moving semi-stationary modes of small horizontal extent correspond to large time-scales.

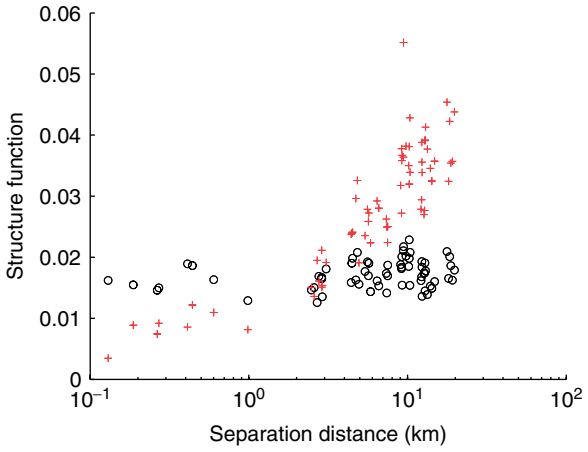

Figure 5. The dependence of between-station (two-point) velocity structure function on station separation distance for the 1 min mode (black circles) and the 32 min mode (red crosses) for the Iowa network.

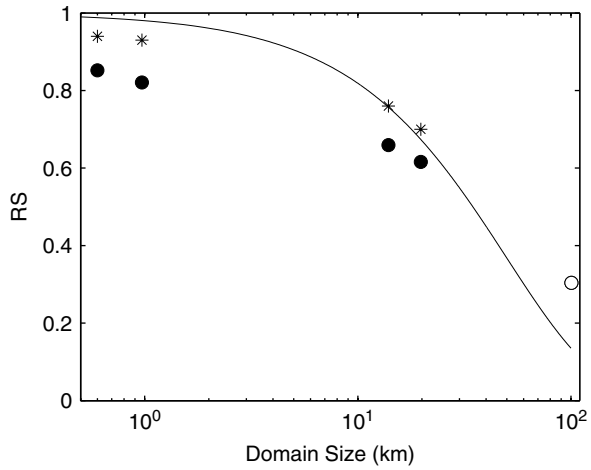

Figure 6. Dependence of RS on network size for the five above-canopy networks, where RS is the ratio of time variability of the spatially averaged flow to the spatial average of the time variability at individual stations. The values of RS are based on 1 min averages (filled circles), 10 min averages (asterisks) and 5 min averages for the Utah data (open circle). For reference, the line represents exponential decay with a $1/e$ folding depth of 50 km.

DOI: 10.1002/qj

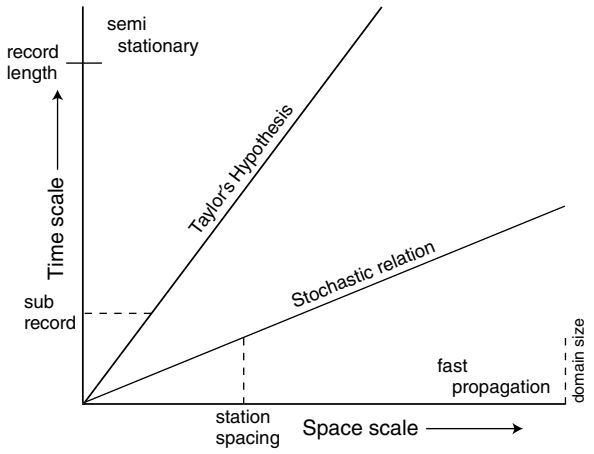

Figure 7. Schematic diagram of regimes in the time–space domain. In this study, the record length is 64 min and the subrecord length is 1 min. Station spacing and domain size vary by orders of magnitude between the networks in the present study. The slope of the line for Taylor's hypothesis is the inverse of the wind speed. Also shown is the time–space stochastic relationship in Section 4.3 where the velocity scale is greater than the wind speed (smaller slope).

We now examine the between-record relationship between the spatial and time variability for the 4 min mode (Figure 8). Time-scales less than 4 min are characterized by smaller spatial coherence while larger time-scales are characterized by insufficient samples to estimate V_{meso} for individual records. A relationship between the strength of spatial variability represented by V_{Domain} (Section 3) and time variability represented by V_{meso} is evident for the Iowa network, but characterized by large scatter (Figure 8). This between-record relationship is stronger for the smaller CASES99 and Young Pine networks, where the spatial coherence of the 4 min mode is better resolved. This relationship is weaker for the Utah network where the station spacing is large. The large between-record scatter in the space–time relationship for all of the networks indicates that greater time variability does not necessarily imply greater space variability, and vice versa.

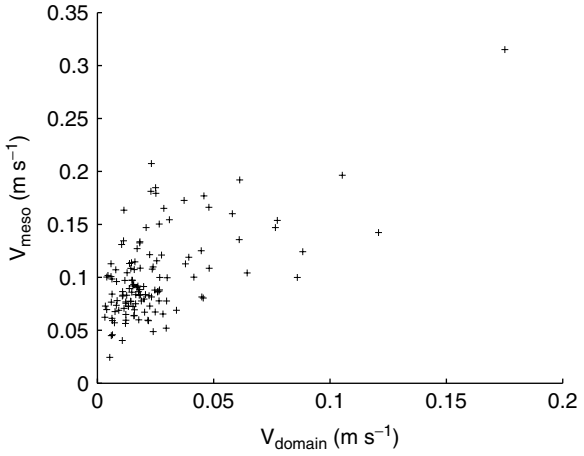

Figure 8. The relationship between the velocity scale representing time variation of the horizontal flow (V_{meso}, (6)) and the velocity scale representing spatial variation (V_{Domain}, (2)) for the 4 min mode in the Iowa network.

7. Conclusions

In this article, we have examined the space–time statistics for mesoscale motions in stable boundary layers using eight networks of wind data. The overall statistics mask the complex variety of mesoscale signatures and thus shed little light on the dynamics of such flows. However, the statistics do reveal new characteristics of mesoscale motions not previously identified. The horizontal scale of spatial coherence increases with increasing time-scale that can be posed in terms of a velocity scale (Section 4.3).

The decrease of between-station coherence with increasing separation distance between stations is more complex than exponential, probably reflecting multiple generation processes. For most of the networks, a significant fraction of the spatial variability is a result of spatial variations that are systematic in time, apparently associated with surface heterogeneity; however, the total spatial variability at a given time is often dominated by transient mesoscale motions.

Spatial variability complicates comparisons of models with observations at a single point. Spatially averaging the observed flow over the network, as a surrogate model grid area, leads to significantly less time variability. Comparing results between networks indicates that the time variability decreases with increasing width of the averaging area, with a rough exponential fit corresponding to a $1/e$ folding depth of the order of 50 km.

A variety of statistical measures reveal that the nature of the mesoscale motions differ substantially between networks, presumably partly because of different surface conditions, general topography and prevailing synoptic regime. Such variations along with multiple generation mechanisms preclude simple similarity theory or detailed conclusions in general for mesoscale motions in the nocturnal boundary layer. Between-network variations may also be influenced by poor spatial resolution and different network configurations.

Future progress will require substantially improved observation networks. Because mesoscale motions are characterized by multiple generation mechanisms, larger time-scales than turbulence and relatively rare strong events, longer observational periods are required, preferable a year or more. Mesoscale motions span a wide range of scales requiring station spacing as small as tens of metres over at least a small part of the network. Measurements of vertical structure at one or more points are required for a meaningful description of such motions. With existing technology, two-dimensional sonic anemometers are preferable to cup and propeller anemometers in order to avoid threshold problems in very weak winds.

Acknowledgements

The valuable comments of the reviewers, Steve Hanna and Danijel Belušić, are greatly appreciated. The Utah data were provided by Alfred Astling, while the EBEX and CASES99 data were provided by the Integrated Surface Flux Facility of the National Center for Atmospheric

DOI: 10.1002/qj

Research. This material is based upon work supported by National Science Foundation Grant ATM-0607842, ARO Contract W911FN05C0067, DTRA grant W911NF-06-1-0439 and DOE Grant DE-FG02-06ER64318.

References

Anderson PS. 2003. Fine-scale structure observed in a stable atmospheric boundary layer by Sodar and kite-borne tethersonde. *Boundary-Layer Meteorol.* **107**: 323–351.

Anfossi D, Oettl D, Degrazia G, Boulart A. 2005. An analysis of sonic anemometer observations in low wind speed conditions. *Boundary-Layer Meteorol.* **114**: 179–203.

Belušić D, Mahrt L. 2008. Estimation of length scales from mesoscale networks. *Tellus A* **60**: 706–715.

Finnigan J, Einaudi F, Fua D. 1984. The interaction between an internal gravity wave and turbulence in the stably-stratified nocturnal boundary layer. *J. Atmos. Sci.* **41**: 2409–2436.

Hanna S. 1983. Lateral turbulence intensity and plume meandering during stable conditions. *J. Clim. Appl. Meteorol.* **22**: 1424–1430.

Hanna S, Chang J. 1992. Representativeness of wind measurements on a mesoscale grid with station separations of 312 m to 10 km. *Boundary-Layer Meteorol.* **60**: 309–324.

Howell J, Mahrt L. 1997. Multiresolution flux decomposition. *Boundary-Layer Meteorol.* **83**: 117–137.

King JC. 1988. Some measurements of length-scales in the stably-stratified surface layer. Pp. 39–53 in *Stably-stratified Flow and Dense Gas Dispersion*, Puttock JS (ed). Oxford University Press: Oxford.

Kustas W, Li F, Jackson J, Prueger J, MacPherson J, Wolde M. 2004. Effects of remote sensing pixel resolution on modeled energy flux variability of croplands in Iowa. *Remote Sensing Environ.* **92**: 535–547.

Lilly DK. 1983. Stratified turbulence and the mesoscale variability of the atmosphere. *J. Atmos. Sci.* **40**: 749–761.

Lindborg E. 1999. Can the atmospheric kinetic energy spectrum be explained by two-dimensional turbulence? *J. Fluid Mech.* **388**: 259–288.

Mahrt L. 2007. Weak-wind mesoscale meandering in the nocturnal boundary layer. *Environ. Fluid Mech.* **7**: 331–347.

Mahrt L. 2008. Mesoscale wind direction shifts in the stable boundary-layer. *Tellus A* **60**: 700–705.

Nakamura R, Mahrt L. 2005. A study of intermittent turbulence with CASES-99 tower measurements. *Boundary-Layer Meteorol.* **114**: 367–387.

Nappo CJ. 2002. *An Introduction to Atmospheric Gravity Waves*. Academic Press: New York.

Oncley SP, Foken T, Vogt R, Kohsiek W, de Bruin H, Bernhofer C, Christen A, van Gorsel E, Grantz D, Lehner I, Liebethal C, Liu H, Mauder M, Pitacco A, Ribeiro L, Weidinger T. 2007. The Energy Balance Experiment EBEX-2000. Part I: Overview and energy balance. *Boundary-Layer Meteorol.* **123**: 1–28.

Panofsky HA, Dutton JA. 1984. *Atmospheric Turbulence: Models and Methods for Engineering Applications*. John Wiley: New York.

Poulos G, Blumen W, Fritts D, Lundquist J, Sun J, Burns S, Nappo C, Banta R, Newsom R, Cuxart J, Terradellas E, Balsley B, Jensen M. 2001. CASES-99: A comprehensive investigation of the stable nocturnal boundary layer. *Bull. Am. Meteorol. Soc.* **83**: 555–581.

Rees J, Anderson P, King J 1998. Observations of solitary waves in the stable atmospheric boundary layer. *Boundary-Layer Meteorol.* **86**: 47–61.

Rees JM, Denholm-Price J, King JC, Anderson PS. 2000. A climatological study of internal gravity waves in the atmospheric boundary layer overlying the Brunt ice shelf. *Antarctica J. Atmos. Sci.* **57**: 511–526.

Schwarz P, Law B, Williams M, Irvine J, Kurpius M, Moore D. 2004. Climatic versus biotic constraints on carbon and water fluxes in seasonally drought-affected ponderosa pine ecosystems. *Global Biochem. Cycles* **18**: 1029–1037.

Shutts G. 1998. Stationary gravity-wave structure in flows with directional wind shear. *Q. J. R. Meteorol. Soc.* **124**: 1421–1442.

Skelly B. 2004. Atmospheric disturbances that generate intermittent turbulence in nocturnal boundary layers. *Boundary-Layer Meteorol.* **110**: 255–279.

Sun J, Lenschow DH, Burns SP, Banta RM, Newsom RK, Coulter R, Frasier S, Ince T, Nappo C, Balsley B, Jensen M, Mahrt L, Miller D, Skelly B. 2004. Atmospheric disturbances that generate intermittent turbulence in nocturnal boundary layers. *Boundary-Layer Meteorol.* **110**: 255–279.

Thomas C, Martin JG, Goeckede M, Siqueira MB, Foken T, Law B, Loescher H, Katul G. 2008. Estimating daytime subcanopy respiration from conditional sampling methods applied to multi-scalar high frequency turbulence time series. *Agric. Forest Meteorol.* **148**: 1210–1229.

Treviño G, Andreas EL. 2006. Dynamical implications of block averaging. *Boundary-Layer Meteorol.* **120**: 497–508.

Vickers D, Mahrt L. 2006. A solution for flux contamination by mesoscale motions with very weak turbulence. *Boundary-Layer Meteorol.* **118**: 431–447.

Vickers D, Mahrt L. 2007. Observations of the cross-wind velocity variance in the stable boundary layer. *Environ. Fluid Mech.* **7**: 55–71.

Yaglom AM. 1973. *Stationary Random Functions*. Dover: New York.

DOI: 10.1002/qj